



UNIVERSITY OF LEEDS

This is a repository copy of *Charging Pattern Optimization for Lithium-Ion Batteries with An Electrothermal-Aging Model*.

White Rose Research Online URL for this paper:
<http://eprints.whiterose.ac.uk/135743/>

Version: Accepted Version

Article:

Liu, K, Zou, C, Li, K et al. (1 more author) (2018) Charging Pattern Optimization for Lithium-Ion Batteries with An Electrothermal-Aging Model. *IEEE Transactions on Industrial Informatics*, 14 (12). pp. 5463-5474. ISSN 1551-3203

<https://doi.org/10.1109/TII.2018.2866493>

(c) 2018 IEEE. Personal use of this material is permitted. Permission from IEEE must be obtained for all other uses, in any current or future media, including reprinting/republishing this material for advertising or promotional purposes, creating new collective works, for resale or redistribution to servers or lists, or reuse of any copyrighted component of this work in other works.

Reuse

Items deposited in White Rose Research Online are protected by copyright, with all rights reserved unless indicated otherwise. They may be downloaded and/or printed for private study, or other acts as permitted by national copyright laws. The publisher or other rights holders may allow further reproduction and re-use of the full text version. This is indicated by the licence information on the White Rose Research Online record for the item.

Takedown

If you consider content in White Rose Research Online to be in breach of UK law, please notify us by emailing eprints@whiterose.ac.uk including the URL of the record and the reason for the withdrawal request.



eprints@whiterose.ac.uk
<https://eprints.whiterose.ac.uk/>

Charging Pattern Optimization for Lithium-Ion Batteries with An Electrothermal-Aging Model

Kailong Liu, *Member, IEEE*, Changfu Zou, *Member, IEEE*, Kang Li, *Senior member, IEEE*, Torsten Wik

Abstract—This paper applies advanced battery modeling and multi-objective constrained nonlinear optimization techniques to derive suitable charging patterns for lithium-ion batteries. Three important yet competing charging objectives, including battery health, charging time, and energy conversion efficiency, are taken into account simultaneously. These optimization objectives are first subject to a high-fidelity battery model that is synthesized from recently developed individual electrical, thermal, and aging models. The coupling relationship and multiple timescales among different model dynamics are identified. Furthermore, constraints are considered explicitly on the current, voltage, state-of-charge, and temperature. Such a complex charging problem is solved by using an ensemble multi-objective biogeography-based optimization (EM-BBO) approach. As a result, two charging patterns, namely the constant current-constant voltage (CC-CV) and multistage constant current-constant voltage (MCC-CV), are optimized to balance various combinations of charging objectives. Different trade-offs and sensitive elements are compared and analyzed based on the Pareto frontiers. Illustrative results demonstrate that the proposed strategy can effectively offer feasible health-conscious charging with desirable trade-offs among charging speed and energy conversion efficiency under different demand priorities.

Index Terms—Electric vehicles, lithium-ion batteries, fast charging, battery charging optimization, electrothermal-aging model.

I. INTRODUCTION

Lithium-ion (Li-ion) batteries have been preferably exploited as energy and power sources to drive electric vehicles (EVs) due to their performance, financial, and environmental superiorities over other candidates, like fuel cells, supercapacitor, lead-acid batteries, and nickel-metal-hydride batteries [?], [1]. However, if compared to internal combustion engines associated with fossil fuels, Li-ion batteries are still inferior in the upfront cost, “refueling” time, driving range, and service life [?]. Although innovations in battery technologies in materials and chemistry may solve the problems in the long

Manuscript received May 19, 2018; revised June 30, 2018; accepted August 14, 2018. This work was supported in part by the UK EPSRC under Grant EP/L001063/1 and in part by the Swedish Energy Agency under Grant 39786-1. Paper no. TII-18-1703. (Corresponding author: Changfu Zou.)

K. Liu is with the Warwick Manufacturing Group, University of Warwick, Coventry, CV4 7AL, United Kingdom (kliu02@qub.ac.uk).

C. Zou and T. Wik are with the Department of Electrical Engineering, Chalmers University of Technology, Gothenburg 41296, Sweden (changfu.zou@chalmers.se, tw@chalmers.se).

K. Li is with the School of Electronic and Electrical Engineering, University of Leeds, Leeds, LS2 9JT, United Kingdom (K.Li1@leeds.ac.uk).

TABLE I
GLOBAL NOMENCLATURE.

Ah	Accumulated current throughput in ampere-hours
C_1, C_2	Capacity of the first and second RC networks
C_c, C_s	Internal and surface heat capacity
C_n	Nominal capacity in ampere-seconds
C_{nloss}	Relative capacity loss of the battery in percentage
E_a	Activation energy
I	Charging current
OCV	Open circuit voltage
Q	Heat generation
R_0	Internal resistance
R_1, R_2	Resistance of the first and second RC networks
R_c, R_u	Heat conduction and convection resistance
R_g	Universal gas constant
T_{amb}	Ambient temperature
T_c, T_s	Core and surface temperature
V	Terminal voltage
V_1, V_2	Voltage of the first and second RC networks

run, mass deployment of EVs into the current market requires an immediate solution [2], [3]. This intuitively motivates the development of intelligent battery management systems, aiming to extract the full potential of batteries.

In addition to the matter of time, charging strategies are influential to energy efficiency and battery aging [4]–[6]. Meanwhile, fast charging can be an effective way to alleviate vehicle range anxiety. Therefore, designing proper charging strategies is one of the most important tasks in battery management systems. This is, however, technically challenging due to three major factors. First, design objectives, including time, energy efficiency, and battery state-of-health, are simultaneously involved, interrelated, and potentially competing with each other. Second, these objectives are subject to a complex battery system, consisting of coupled nonlinear electrical, thermal, and aging dynamics over disperse timescales [7]. Additionally, constraints must be imposed, e.g., on current, voltage, and temperature, to protect the battery from overcharging and overheating along with premature degradation and safety issues.

To address the above challenges, some attempts have been made on the development of charging strategies based on different types of models that monitor and predict in-situ battery states. Physics-based models developed from first principles are gaining increased interest in advanced battery charging management. On the basis of electrochemical models, nonlinear optimization problems were formulated to minimize the charging duration in [8]. Linear-time-varying and nonlinear model predictive control algorithms have recently been proposed for battery charging in [9], [10], where minimum

time problems subject to health-related constraints and electrochemical models were considered. Although attractive charging performance has been demonstrated in the simulation-based environment, this class of strategies is still far from wide practical deployment. This is because that identification and observability studies for first-principle battery models that capture all the coupled nonlinear dynamics are non-trivial tasks. Formal technique tools with provable convergence have not been well established. Furthermore, physics-based battery models that are initially described by nonlinear partial differential equations (see [11] for details) require intensive computational resources and can therefore be overly expensive to implement in real-time.

To overcome the above technical and economic issues, charging strategies based on the equivalent circuit models have been designed. For example, by using a simplified model constituted by an ideal voltage source and an internal resistor, Abdollahi et al. [12] derived an analytical solution to a linear optimization problem for battery charging. Built upon a nonlinear electrothermal-aging model, Perez et al. [13] developed an open-loop optimal controller to balance battery degradation and the charging speed. Based on an electrothermal battery model, Zou et al. [14] formulated a constrained predictive control problem to reduce charging time and suppress temperature increase. Besides, multi-objective optimization techniques have also been applied in battery charging management. Hu et al. [15] formulated a dual-objective optimization problem for battery charging based on a first-order resistor-capacitor model, where the pseudo-spectral technique was employed to minimize the charging time and energy loss. In [16], a specific optimization problem considering charging time and battery temperature was formulated based on an enhanced thermal behavior model, then the genetic algorithm was used to optimize charging current. Liu et al. [17] formulated a multi-objective function to consider both surface and internal temperature rises during charging, then a heuristic method named Teaching-learning-based-optimization along with a coupled thermoelectric model was applied to search the optimal charging profile. By designing a modified isolated buck converter based on a Rint battery model, a two-layer charging approach was developed to schedule the charging current profile by considering user demand, cell equalization and temperature effects in [18]. These referred works appear to be promising for scheduling battery charging. However, they partially addressed the charging problem by accounting for a subset of the objectives and battery dynamics, potentially leading to sub-optimal solutions.

Charging approaches with predefined profiles are adopted widely in the battery industry due to their reliability, simplicity, and cost-effectiveness. The most well-known charging pattern is constant current-constant voltage (CC-CV) [19]. In this approach, a battery is charged by a constant current (CC) first until its terminal voltage rises up to a predefined threshold. Then, the battery starts to be charged with a constant voltage (CV), entailing the continuous step-down of the charging current. Another popular charging pattern, named multistage constant current-constant voltage (MCC-CV), consists of several CC phases with decreased current rates and a CV phase in the

end [19]. For these approaches, tuning the parameters, such as current rates and voltage thresholds, can influence the charging performance significantly [20]. Trial-and-error methods for different charging protocols have been performed in [19]. With the maximum charging capacity as the main objective, the Fuzzy-control approach [21] and Taguchi method [22] were used to search optimal charging patterns. However, these algorithms have not explicitly considered battery internal real-time information especially aging state and consequently, the obtained solutions are heuristic.

In this regard, model-based optimization algorithms are exploited to find the optimal tuning parameters for CC-CV and MCC-CV charging patterns. Biogeography-based optimization (BBO) is a powerful specialized technique tool proposed by Simon et al. [23] for handling complex optimization problems. Many variants of BBO have been applied successfully in industrial applications, thanks to their fast convergence performance and being free of parameter tuning [24]. Therefore, for battery management, BBO may be a good candidate to search for proper charging.

Based on the above discussions, this paper applies advanced battery modeling and multi-objective optimization technologies to derive the suitable CC-CV and MCC-CV patterns, enabling satisfactory trade-offs among key but contradictory charging objectives of Li-ion batteries under different demand priorities. Specifically, three key original contributions are made in this paper. First, crucial charging objectives in terms of charging time, battery aging, and energy loss are sequentially formulated for battery charging operation. These objectives are subject to a high-fidelity electrothermal-aging model and hard constraints imposed on the system's physical variables. Next, as the battery charging optimization involving coupled highly nonlinear dynamics over different timescales is a very complex process, a framework based on the EM-BBO approach is developed to efficiently search charging patterns that can optimally trade-off these conflicting objectives. Finally, due to the fact that the Pareto frontier provides a set of optimal solutions that can be presented graphically to demonstrate the conditions where one situation cannot be improved without making another situation worse, any resultant CC-CV and MCC-CV patterns can be compared graphically by using the Pareto frontiers. The effects of sensitive elements on the optimization results are also analyzed. It is worth noting that the proposed algorithm is readily extendable to other battery types with suitable models.

The remainder of this paper is structured as follows. Section II presents the electrothermal-aging battery model. Based on this model, different charging patterns and optimization objectives are formulated in Section III. The model-based optimization procedure for charging patterns is proposed in Section IV and then implemented in Section V, followed by concluding summaries of this work in Section VI.

II. BATTERY ELECTROTHERMAL-AGING MODEL

Various mathematical models have been developed to capture battery behaviors. For instance, comprehensive studies have been performed in [25] for different electrical models

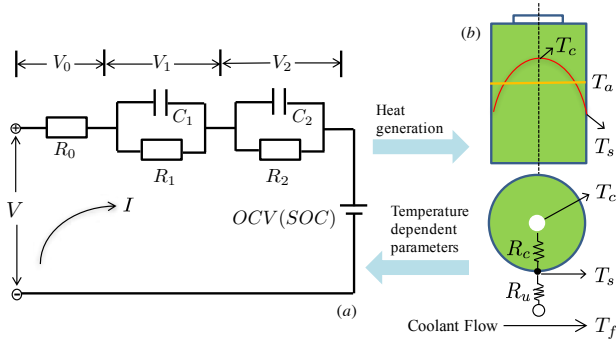


Fig. 1. An electrothermal model for a lithium-ion battery [14]. (a) The equivalent circuit electrical model. (b) A lumped thermal model.

and in [26] for battery aging models. This study considers a complete battery model synthesized from a second-order resistor-capacitor (RC) electrical model, a two-state lumped thermal model [27], and a capacity loss model [28].

1) *Battery electrothermal model.* The diagram of coupled electrothermal battery model is shown in Fig 1. By using the notations defined in Table I, this electrothermal model can be mathematically given by:

$$\frac{dSOC(t)}{dt} = \frac{I(t)}{C_n} \quad (1a)$$

$$\frac{dV_1(t)}{dt} = \frac{V_1(t)}{R_1(t)C_1(t)} + \frac{I(t)}{C_1(t)} \quad (1b)$$

$$\frac{dV_2(t)}{dt} = \frac{V_2(t)}{R_2(t)C_2(t)} + \frac{I(t)}{C_2(t)} \quad (1c)$$

$$\frac{dT_s(t)}{dt} = \frac{T_{amb} - T_s(t)}{R_u C_s} - \frac{T_s(t) - T_c(t)}{R_c C_s} \quad (1d)$$

$$\frac{dT_c(t)}{dt} = \frac{T_s(t) - T_c(t)}{R_c C_c} + \frac{Q(t)}{C_c} \quad (1e)$$

where V_1 describes the voltage due to the charging transfer process, and V_2 is the voltage to reproduce battery diffusion process. In (1e), the heat generation $Q(t)$ is governed by:

$$Q(t) = I(t)T_c(t) \frac{dOCV(t)}{dT_c(t)} + I(t)(V(t) - OCV(t)) \quad (2)$$

The first term on the right-hand side of (2) is the heat generated by the entropy change, and the second term stands for the Joule's heating. The open circuit voltage $OCV(t)$ have a nonlinear relation with the SOC level. The terminal voltage $V(t)$ is defined as:

$$V(t) = OCV(SOC(t)) + R_0(t)I(t) + V_1(t) + V_2(t) \quad (3)$$

It is worth noting that battery electrical and thermal characteristics in the model (1)-(3) are strongly coupled. To be specific, parameters in RC pairs (e.g., R_1, C_1, R_2 , and C_2) are time-varying and dependent on $SOC(t)$ and $T_c(t)$. Meanwhile, the resistance $R_0(t)$ will be appreciably influenced by the battery core temperature $T_c(t)$. It is evident from (2) that the heat generation $Q(t)$ is also affected by the electrical dynamics.

In this study, cylindrical 26650 lithium iron phosphate (LiFePO_4) cells are adopted, and each of them has a 3.3 V

nominal voltage. These battery cells are capable of offering long cycle life with a small impedance increase. For example, at 25°C, more than 5000 full depth of discharge (DOD) cycles can be delivered before the battery's capacity reduces to its end of life (EOL). The calibration technique and corresponding parameters of the battery electrothermal model can be found in [27].

2) *Battery aging model.* For Li-ion battery charging operation, the cycle life rather than calendar life is focused on. In this study, the accumulation effects of ampere-hour (Ah) throughput on the battery capacity degradation are captured by a cycle-life model based on the Arrhenius equation in the form [28]:

$$C_{nloss}(f, Ah) = \delta_{func}(f) \times Ah^z \quad (4)$$

where f stands for the set of charging stress factors to cause battery aging, z is a power law parameter, and $\delta_{func}(f)$ is a nonlinear function to capture the effects of charging factors on battery aging phenomena. Here the Ah throughput represents the amount of charge delivered by both charging and discharging during battery cycling operation. This Ah throughput model has been shown to have a powerful capability to capture the effects of charging behavior on the battery capacity loss [29]. The factors influencing battery degradation are multiple and complex, and their characterization and quantification are an actively ongoing research topic for Li-ion batteries. For charging operation where voltage bounds are often imposed, the charging current rate, SOC, and average temperature are the three key factors accelerating a battery's aging. For the validation of this aging model, according to Suri and Onori [28], data can be specified in terms of average current rate, average SOC, and average battery temperature for three different cycle cases. By these authors, $\delta_{func}(f)$ in such a model has been further expressed as:

$$\delta_{func}(f) = (\alpha \cdot \bar{SOC} + \beta) \cdot \left[\frac{-E_a + \eta \cdot \bar{I}_c}{R_g \cdot (273.15 + \bar{T}_b)} \right] \quad (5)$$

where α and β are the parameters to reflect the effects of battery SOC, and η defines the current dependence. \bar{SOC} , \bar{I}_c and \bar{T}_b are specified in terms of average battery SOC, average current rate and average battery temperature during one cycle. Parameters of this battery aging model should be identified using experimental cycling data. A detailed identification process is referred to [28] and not provided here for brevity. This validated aging model presents a satisfactory result to describe the battery capacity degradation during cycling operation. The values of α and β at different SOC levels are given in Table II. Battery degradation also has a strong coupling relationship with the electrothermal dynamics. The degraded capacity will be predicted by this aging model, based on which the specific aging objective can be formulated.

3) *Coupled electrothermal-aging model.* The complete battery model describing the electrothermal-aging phenomena has been presented. All the variables are divided into two parts with different timescales. In the fast timescale associated with electrothermal dynamics and a time index t , the corresponding variables are defined as the input vector $u(t) := I(t)$, the output vector $y(t) := [V(t), R_0(t), R_1(t), R_2(t)]^T$, and the

TABLE II
VALUES OF α AND β AT DIFFERENT SOC LEVELS [28].

Parameters	$SOC < 0.45$	$SOC \geq 0.45$
α	2897.8	2694.3
β	7413.1	6025.6

state vector $x(t) := [SOC(t), V_1(t), V_2(t), T_c(t), T_s(t)]^T$. In the slow timescale, the time index τ is used to indicate the τ -th charging cycle. After obtaining the average SOC level, average C-rate, average battery temperature, and Ah throughput over the τ -th charging cycle as $\bar{SOC}(\tau)$, $\bar{I}_c(\tau)$, $\bar{T}_b(\tau)$, and $Ah(\tau)$, respectively, the battery's capacity loss can be predicted based on (4)-(5). The corresponding variables are $u_a(\tau)$ and $y_a(\tau)$ that stand for the input and output vectors of the aging model, respectively. Based on these definitions, the obtained battery model (1)-(5) can be re-written in a compact form:

$$\dot{x}(t) = A(t)x(t) + B(t)u(t) \quad (6a)$$

$$y(t) = h(x(t), u(t)) \quad (6b)$$

$$u_a(\tau) = [S\bar{O}C(\tau), \bar{I}_c(\tau), \bar{T}_b(\tau), Ah(\tau)]^T \quad (6c)$$

$$y_a(\tau) = C_{nloss}(S\bar{O}C(\tau), \bar{I}_c(\tau), \bar{T}_b(\tau), Ah(\tau)) \quad (6d)$$

where both $A(t)$ and $B(t)$ are time-varying matrices. For a given charging pattern and initial battery states, the transient terminal voltage, SOC, and surface/core temperatures during the charging process can be predicted recursively according to (6). Based on the obtained fast state $x(t)$, u_a can be calculated and is further selected as the input for the aging model to predict the battery capacity loss y_a caused by this specific charging pattern.

III. CHARGING PATTERNS AND OBJECTIVES DESIGN

Based on the battery model obtained in the previous section, model-based algorithms can be developed to optimize charging patterns regarding various charging objectives.

1) *Charging patterns.* The first charging pattern to be optimized for Li-ion batteries is CC-CV, as shown in Fig. 2(a). The key factors in such a CC-CV charging pattern are the current rate I_{cc} in a CC stage and the voltage value V_{cv} in a CV stage. For the most extensively used Li-ion batteries, V_{cv} is generally set as the maximum cut-off voltage to improve battery capacity utilization. For I_{cc} , on the one hand, the battery's charging time can be shortened by using a large I_{cc} , but this may lead to serious lithium plating, low efficiency of energy conversion, and overheating. All these phenomena have significant effects on the battery service life. Namely, the saved time may be achieved at the sacrifice of battery state-of-health. Therefore, it is imperative to carry out appropriate current rates in the CC-CV pattern to not only speed up the battery charging process but also suppress the battery's degradation.

The second type of charging patterns is MCC-CV shown in Fig. 2(b). The open problem for using MCC-CV charging patterns is to set the appropriate values of various currents ($I_{C1} > I_{C2} > \dots > I_{CN}$) and voltages (V_{boost} and V_{ch}). The charging speed of MCC-CV patterns is mainly determined by the number of CC stages and their corresponding current rates. It should be noted that I_{C1} needs to be large enough to achieve

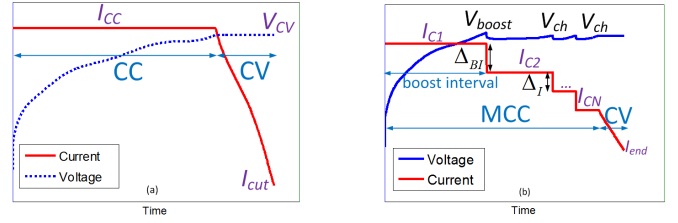


Fig. 2. Current and voltage profiles for CC-CV and MCC-CV patterns.

quick charging throughput within the boost interval. This stage is ended when the terminal voltage reaches V_{boost} . A large cut-off voltage V_{ch} is generally adopted to guarantee utilization of battery capacity. The similar rules for adjusting the battery degradation and energy conversion efficiency as for CC-CV patterns can also be applied to optimize MCC-CV charging patterns.

2) *Charging objectives.* To charge the batteries fast, energy-efficiently, and healthily, the charging speed, energy conversion efficiency, and battery aging are explicitly considered as the optimization objectives.

For the battery charging speed, a faster charging pattern intuitively means that less time is required in the total charging process. The cost function J_{CT} for battery charging time (CT) is easily expressed as:

$$J_{CT} = \Delta t \cdot t_{CT} \quad (7)$$

where Δt signifies the sampling time for digital system implementation, and t_{CT} is the aggregated sampling number when the battery is charged from an initial SOC to its target value. Δt relates to t according to $k\Delta t = t$ and $k = 1, \dots, t_{CT}$.

For the battery energy conversion, higher efficiency of energy conversion means less energy loss occurred in the total charging process. The cost function J_{EL} for energy loss (EL) is described as:

$$J_{EL} = \Delta t \sum_{t=0}^{t_{CT}} \left[R_0(t)I^2(t) + \frac{V_1^2(t)}{R_1(t)} + \frac{V_2^2(t)}{R_2(t)} \right] \quad (8)$$

where all the elements such as resistances and voltages in this function can be obtained from the battery model (6).

In EV applications, the EOL of Li-ion batteries is generally set as the cycle number or throughput when the capacity loss reaches 20% of its nominal capacity. Assuming the battery is charged by the same pattern to finish the same task in each cycle, the maximum battery life by using this specified charging pattern can be calculated through:

$$Ahtotal = [20/\delta_{func}(S\bar{O}C, \bar{I}_c, \bar{T}_b)]^{1/z} \quad (9)$$

where $Ahtotal$ represents the maximum battery life, i.e. the corresponding total charging throughput in Ah, which is affected by the $S\bar{O}C$, \bar{I}_c , and \bar{T}_b of the selected charging pattern. For the battery aging objective, the charging throughput in each charging cycle is an accumulated value and can be expressed as:

$$Aheach = \frac{1}{3600} \int_0^{t_{CT}} I(t)dt \approx \frac{\Delta t}{3600} \sum_{t=0}^{t_{CT}} I(t). \quad (10)$$

Then, the cost function J_{BA} for battery aging (BA) is formulated in the following form as:

$$J_{BA} = A_{each}/A_{total} \quad (11)$$

where J_{BA} represents the reciprocal of the charging cycle number by using the specified charging pattern. It is easy to know that a smaller value of J_{BA} gives the battery a longer service life.

Once the charging pattern is optimized by an appropriate approach built on the battery electrothermal-aging model, all the elements of the three objective functions in (7)-(11) can be obtained. As the input to the dynamic system, the current plays a vital role in optimizing charging patterns and therefore is selected as the decision variable to be optimized for achieving health-conscious charging.

IV. OPTIMAL BATTERY CHARGING STRATEGY

In this section, a novel model-based optimization algorithm, subject to the model in Section II and the objectives in Section III, is formulated to derive optimized charging patterns for Li-ion batteries.

For the MCC-CV pattern, the current $I_{CV}(t)$ at the CV stage can be expressed as:

$$I_{CV}(t) = [V_{ch} - V_1(t) - V_2(t) - OCV(t)]/R_0(t). \quad (12)$$

The voltage V_{boost} in the boost interval is generally equal to or slightly larger than the cut-off voltage V_{ch} [19]. When the input current profile is determined, all the battery electrical and thermal behaviors can be reproduced by the electrothermal model. Then, the associated aging dynamics can also be predicted from (6c)-(6d).

The goal to search suitable MCC-CV charging patterns can be formulated as the following nonlinear constrained optimization problem:

Minimize and equilibrate charging objectives: J_{CT} , J_{EL} , and J_{BA} ,

Subject to: The battery model (6) and operation constraints:

$$SOC_0 \leq SOC(t) \leq SOC_{tCT} \quad (13a)$$

$$I_{\min} \leq I(t) \leq I_{\max} \quad (13b)$$

$$V_{\min} \leq V(t) \leq V_{\max} \quad (13c)$$

$$V_{\min} \leq V_{ch} \leq V_{boost} \leq V_{\max} \quad (13d)$$

$$T_{s,\min} \leq T_s(t) \leq T_{s,\max} \quad (13e)$$

where SOC_0 and SOC_{tCT} are the battery's initial and target SOC levels, I_{\min} and I_{\max} are the minimum and maximum charging currents, V_{\min} and V_{\max} stand for the thresholds of battery terminal voltage, $T_{s,\min}$ and $T_{s,\max}$ are the highest and lowest permissible temperatures for battery effective cycling operation and safety. By (13d), both V_{boost} and V_{ch} are bounded within the range of allowable voltages.

The CC-CV charging pattern can be regarded as a special case of MCC-CV, where only one CC stage and one CV stage are incorporated. The optimization of CC-CV/MCC-CV charging patterns is a complex task due to at least the following four facets: 1) many elements, such as resistances and

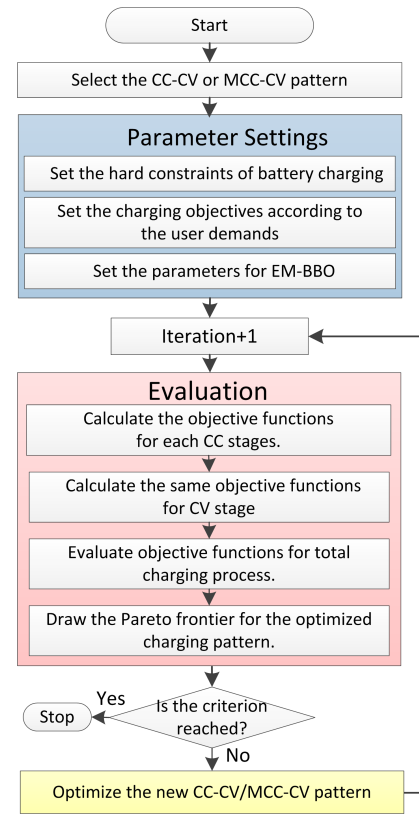


Fig. 3. The procedure to optimize CC-CV/MCC-CV charging patterns based on EM-BBO.

capacitances in the battery's electrothermal model, are time-varying parameters dependent on the SOC and temperature; 2) the relations of capacity loss and battery electrothermal dynamics exist in a highly nonlinear form; 3) hard constraints need to be carefully considered in the optimization process; and 4) proper trade-offs between various objectives during battery charging need to be manipulated meticulously. These bring significant challenges for optimization tools and call for effective optimization approaches to search for charging patterns with the ability to optimally equilibrate conflicting objectives.

As reviewed in the introduction, EM-BBO can be a good candidate to solve the battery charging optimization problem. In the following, an ensemble multi-objective BBO (EM-BBO) approach adopted from [24] is used for battery charging pattern optimization. Rather than a sole BBO approach, four latest improved BBO variants are combined in parallel population to derive this EM-BBO approach. In particular, the individuals of EM-BBO are always updated by the more appropriate BBO approach, resulting in better optimization performance than the sole BBO approach. The detailed calculation process of this method is elaborated in [24]. Here, the emphasis is placed on the EM-BBO implementation procedure for optimization of CC-CV and MCC-CV patterns, as illustrated in Fig. 3. This procedure is further explained in a four-step process as follows:

Step 1: Set the parameters for battery charging. The detailed parameters are the initial and terminal SOC levels: SOC_0 and

SOC_{tCT} ; hard constraints: I_{\min} , I_{\max} , V_{\min} , V_{\max} , $T_{s,\min}$, and $T_{s,\max}$; and the number of CC stages, where CC-CV has one CC stage.

Step 2: Set the charging objectives. Various user demands will lead to a different emphasis on the charging objectives. Select the suitable combination of the key but conflicting objectives based on the user requirements.

Step 3: Set design parameters for the EM-BBO approach: the generation number and initial parallel population sizes. Set the parameters for the battery electrothermal-aging model.

Step 4: For $j = 1$ to j_{\max} do

1) Calculate the objective functions for CC stages until the number of CC stages is reached. One CC stage will transfer to another CC stage as the terminal voltage rises to the voltage threshold.

2) Calculate the same objective functions for the CV stage until the battery SOC reaches its target SOC_{tCT} .

3) Evaluate the objective functions J_{CT} , J_{EL} , and J_{BA} for the total charging process by combining each function terms in all the CC stages and CV stage. Then, the corresponding Pareto frontier for the optimized charging pattern can be formulated.

4) Optimize the CC-CV/MCC-CV pattern by the EM-BBO approach. When the stop criterion j_{\max} is reached, the optimization process will be stopped.

By using this procedure, both the CC-CV and MCC-CV patterns can be optimized to achieve battery health-conscious charging. Meanwhile, other crucial but probably conflicting charging objectives will also be minimized and equilibrated.

V. RESULTS AND DISCUSSIONS

In this section, comparisons of different optimization approaches are conducted first to examine the performance of EM-BBO. Then, the optimization results of CC-CV patterns are presented, followed by four tests to quantify the effects of several key parameters on the optimization results of MCC-CV patterns. A comparison between the CC-CV and MCC-CV charging is also carried out to investigate their efficacies for battery fast health-conscious charging. In these tests, Δt is set as 1s. The Li-ion battery is charged from an initial state $SOC_0 = 0.1$ to the target $SOC_{tCT} = 0.95$. Both the ambient temperature and initial battery temperature are set to be 25°C . The constraints in (13b)-(13e) are specified as: $I_{\min} = 0\text{A}$, $I_{\max} = 15\text{A}$, $V_{\min} = 3.0\text{V}$, $V_{\max} = 3.6\text{V}$, $T_{s,\min} = 5^\circ\text{C}$, and $T_{s,\max} = 45^\circ\text{C}$.

A. Comparisons of optimization approaches

To evaluate the EM-BBO performance, four popular optimization approaches used in the battery domain, including vector evaluated BBO (VE-BBO), non-dominated sorting BBO (NS-BBO) [24], non-dominated sorting genetic algorithm II (NSGA-II) [30], and multi-objective particle swarm optimization (MOPSO) [31], are compared first for different combinations of two charging objectives. All optimization approaches are programmed in Matlab with a 2.40 GHz Intel Pentium 4 CPU. The loop-based, scalar-oriented codes have

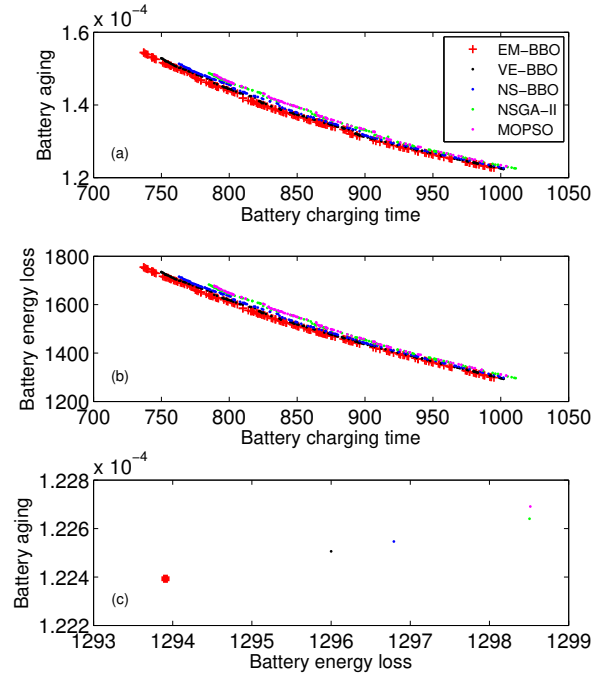


Fig. 4. Optimization results of EM-BBO, VE-BBO, NS-BBO, NSGA-II, and MOPSO for dual objectives.

been revised by using Matlab matrix and vector operations during programming. Besides, multiple parallel subpopulations have also been applied to reduce the computational effort. More details on improvements of computation efficiency are furnished in [24]. Here, the initial parallel population sizes of EM-BBO are all set to the same number N_p . The values of N_p and the generation number G_m are 300 and 50, respectively, for all optimization approaches. For BBO, parameters are self-adaptive adjusted based on the fitness value [24]. For NSGA-II, the mating pool size is set as 0.5 of the whole population, the mutation probability and crossover probability are selected as 1/3 and 0.9, respectively. For MOPSO, the weighting parameter is decreased linearly from 0.4 to 0.2, while the velocity limit parameter is set as 0.5. All the above parameter settings are suggested by the existing publications [30], [31]. The optimization results derived from the five approaches are compared in Fig. 4 in terms of different combinations of two objectives.

It is evident that both the objectives of battery aging and energy loss are contradictory with the charging speed. In Fig. 4(a)-(b), the Pareto frontiers obtained from EM-BBO are much closer to the origin of the rectangular coordinates, indicating that smaller objective values can be achieved. Besides, for NSGA-II and MOPSO, the optimal solution sets are far away from the origin. The corresponding particles are distributed in the narrow regions, which implies that enough information can hardly be presented to the decision makers. Therefore, these two approaches are not suitable for solving the charging optimization problem. For NS-BBO and VE-BBO, the optimal solution sets move towards the left-down, but the particles still converge into relatively small areas. This means that the whole Pareto frontier cannot be reached in

TABLE III
THE RESULTS OF DIFFERENT OPTIMIZATION ALGORITHMS REGARDING
THE MINIMUM VALUES OF J_{CT} , J_{EL} , J_{BA} , ALONG WITH M-IGD,
V-IGD AND T_m .

Methods	J_{CT}	J_{EL} [10^3]	J_{BA} [10^{-4}]	M-IGD [10^{-3}]	V-IGD [10^{-6}]	T_m
True	732	1.294	1.223	–	–	–
EM-BBO	732	1.294	1.224	2.65	3.91	168.26
VE-BBO	749	1.296	1.225	3.14	6.82	273.48
NS-BBO	762	1.297	1.226	3.88	6.72	319.39
NSGA-II	781	1.299	1.227	5.79	7.46	191.62
MOPSO	783	1.301	1.229	5.91	7.38	224.38

NS-BBO and VE-BBO. In contrast, the Pareto frontiers of EM-BBO stretch so long that a variety of optimal solutions are achieved.

In order to give quantitative assessments for the converging performance of implemented optimization approaches, the inverted generational distance (IGD) defined in (14) and the time metric T_m representing the average running time, have been utilized as performance indicators in this study.

$$IGD = \frac{\sum_{i \in P_a} d(i, P_a^*)}{|P_a^*|} \quad (14)$$

where P_a stands for the obtained Pareto frontier. P_a^* is the solution set of the best distributed Pareto frontier. $d(i, P_a^*)$ means the minimum Euclidean distance between i and P_a^* . $|P_a^*|$ represents the cardinality of P_a^* . IGD has been justified as an effective metric to evaluate the convergence and spread performance in many real-world multi-objective optimization applications [32] and is hence adopted in this work. A smaller value of IGD implies better converging performance of a multi-objective optimization algorithm.

Table III shows comparative results for the minimum values of the three objective functions, along with the mean values of IGD (M-IGD), variance values of IGD (V-IGD) and T_m , corresponding to five multi-objective optimization methods. 20 independent runs are performed for each optimization problem. The average fitness values by using the single-objective BBO are set as the true criteria to judge the optimization results. Clearly, the minimum values of J_{CT} , J_{EL} , and J_{BA} calculated from EM-BBO are all closer to the true criteria than other optimization methods. It is also evident that all listed BBO approaches achieve lower values of IGD in Table III, which means that they can easily converge to the uniformly distributed Pareto frontier. The M-IGD and V-IGD for EM-BBO are just 2.65×10^{-3} and 3.91×10^{-6} respectively, which are significantly better than other counterparts. Besides, EM-BBO also presents a competitive performance in terms of running time T_m . This is mainly due to the distinctive migration behavior and ensemble learning ability of EM-BBO. Accordingly, it can be concluded that EM-BBO presents more efficient convergence performance in optimizing the charging patterns whilst equilibrating these different charging objectives.

Interestingly, from Fig. 4(c), all the optimal solutions are just single points. Physically, this phenomenon means that the energy conversion efficiency and battery aging have no conflicts with each other.

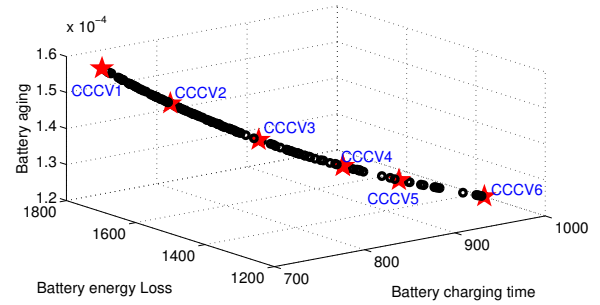


Fig. 5. Pareto frontier obtained by solving the three-objective optimization problem for the CC-CV pattern.

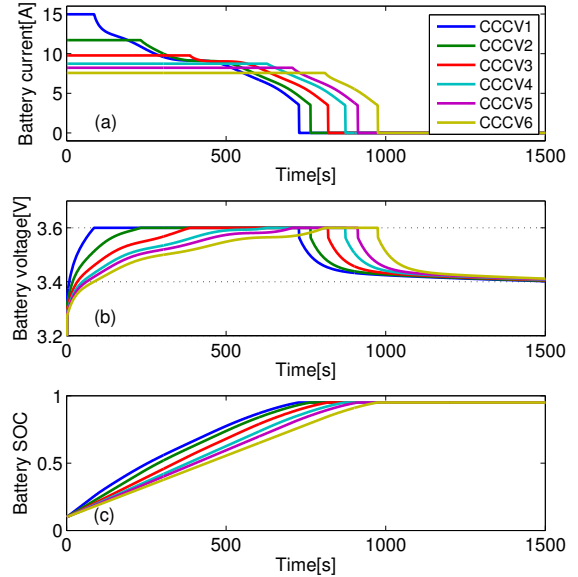


Fig. 6. Charging profiles for the selected CC-CV cases.

B. CC-CV Optimization

We first investigate results by using the EM-BBO approach to optimize the CC-CV charging pattern. The upper voltage threshold for the CV stage is set as $V_{cv} = 3.6V$ according to specifications provided by the battery's manufacturer.

Considering J_{CT} , J_{EL} , and J_{BA} as the optimization objectives simultaneously, the corresponding Pareto frontier is shown in Fig. 5. Six cases from the optimal CC-CV set are selected randomly, and their charging dynamic profiles in terms of current, terminal voltage, and SOC are compared in Fig. 6. It can be readily found that the constant current in CCCV1 is the largest one, i.e. 14.98A. This has caused the terminal voltage to rapidly reach the upper voltage threshold, followed by a long CV stage with the gradually reduced charging current. As a result, the CCCV1 has the shortest charging time, i.e. $J_{CT} = 728$, but the highest energy loss ($J_{EL} = 1.778 \times 10^3$) and battery aging ($J_{BA} = 1.562 \times 10^{-4}$). On the contrary, as the I_{CC} decreases down till the minimum value in CCCV6, the J_{CT} will become larger together with the lower J_{EL} and J_{BA} . Quantitatively, as compared to the conditions of CCCV1, the charging time increases to 976s (34.1% increase) whereas the energy conversion efficiency and

TABLE IV
DETAILED PARAMETERS FOR THE SELECTED MCC-CV CASES WITH VARIOUS CURRENT DECREMENTS.

Cases	Δ_{BI}	Δ_I	J_{CT}	$J_{BA}[10^{-4}]$	$J_{EL}[10^3]$
Case1	1.505	1.004	829	1.383	1.539
Case2	1.640	1.141	834	1.379	1.531
Case3	1.842	1.020	839	1.376	1.525
Case4	1.964	1.162	844	1.371	1.517
Case5	1.999	1.499	850	1.368	1.511

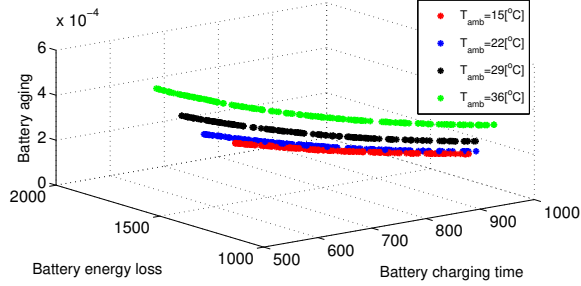


Fig. 10. Pareto frontier for the MCC-CV with different ambient temperatures.

the smallest battery aging ($J_{BA} = 1.368 \times 10^{-4}$) and energy loss ($J_{EL} = 1.511 \times 10^3$) can be achieved at the expense of the largest charging time ($J_{CT} = 850$ s). Based on these results, it can be concluded that by using small current decrements, the charging speed can be enhanced whereas the energy loss and battery degradation would be aggravated.

4) *Effects of ambient temperature.* The ambient temperature T_{amb} also plays an important role in the charging process through heat convection governed by (1d). To quantitatively investigate its impact, the MCC-CV optimization problems are performed under four different values of T_{amb} , i.e. 15°C , 22°C , 29°C , and 36°C .

The optimization results relating to different ambient temperatures are illustrated in Fig. 10. Clearly, a larger ambient temperature results in the Pareto frontier moving to the upper, namely more battery capacity degradation occurs. The ranges of Pareto frontiers become wider by increasing ambient temperatures. Quantitatively, compared to the case with the lowest temperature $T_{amb} = 15^\circ\text{C}$, the minimum charging time of the charging pattern calculated at $T_{amb} = 36^\circ\text{C}$ reduces to 553s, corresponding to a 24.9% decrease; whereas the energy loss and battery aging are $J_{EL} = 1.655 \times 10^3$ and $J_{BA} = 5.023 \times 10^{-4}$, which are 31.9% and 225.3% more than its lowest temperature counterpart. Not surprisingly, increasing T_{amb} will lead to reduced charging time but aggravated energy loss and capacity degradation.

D. Comparisons of CC-CV and MCC-CV Patterns

The analysis in Subsections V-B and V-C has justified that the electrothermal characteristics have significant impacts on optimization results of charging patterns. To further evaluate the efficacies of CC-CV and MCC-CV patterns, comparisons of their optimized solutions for battery health-conscious fast charging are carried out. In the MCC-CV optimization problem, the number of CC stages is specified as 4 and candidate

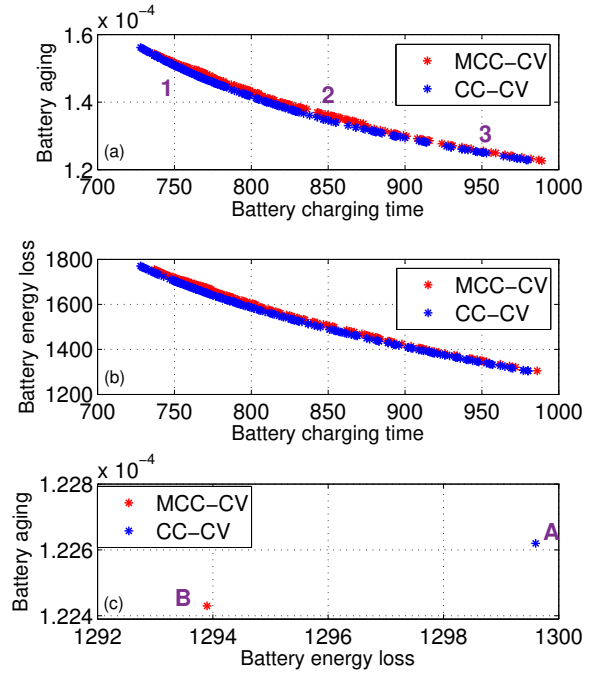


Fig. 11. Comparisons for the Pareto frontiers of the CC-CV and MCC-CV with dual objectives.

pools of initial current increments are set as $\Delta_{BI} \in [1.5, 2]\text{A}$ and $\Delta_I \in [1, 1.5]\text{A}$. Other parameters are the same for both of them, namely, V_{ch} is fixed as 3.6V, and the candidate pool for initial current is set within 7.5A and 15A.

By executing the EM-BBO algorithm with two optimization objectives at each time, the obtained Pareto frontiers are depicted in Fig. 11. From Fig. 11(a)-(b), it is seen that the Pareto frontier for the CC-CV pattern is closer to the origin for both the trade-offs between charging time and aging, and the trade-offs between charging time and energy loss. Three cases corresponding to charging times of 750s, 850s, and 950s in the Pareto frontiers are selected for further analysis. For these cases, their dynamic charging profiles and the associated characteristic parameters are provided in Fig. 12 and Table V, respectively. Quantitatively, the initial constant currents in the cases of MCC-CV1, MCC-CV2, and MCC-CV3 are 13.571A, 9.684A, and 7.895A, respectively, which are over 8%, 7%, and 1% more than their corresponding CC-CV counterparts. The additional time required by MCC-CV patterns mainly compensates for stepwise decreased currents along the CC stages. When the charging time is the same for MCC-CV and CC-CV patterns, the battery aging J_{BA} in the optimization solution set for the former pattern is always slightly larger than that of the later. With the same SOC change, namely the same $\bar{S}\bar{O}\bar{C}$, such a difference is mainly due to a large average current \bar{I}_c used in the MCC-CV pattern associated with a high average battery temperature \bar{T}_b . Meanwhile, because more electric energy has been transformed into heat, MCC-CV suffers from relatively low energy efficiency.

The Pareto frontiers, originated from a dual-objective optimization problem concerning energy loss and battery aging,

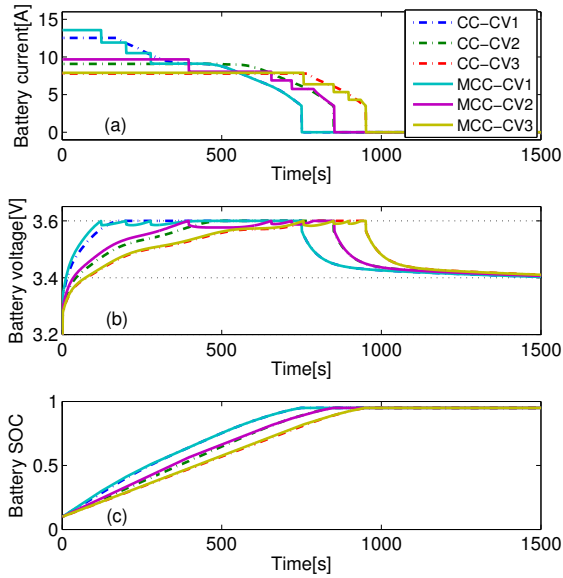


Fig. 12. Charging profiles for the optimized CC-CV and MCC-CV cases focus on speed and battery aging.

TABLE V
CHARACTERISTIC PARAMETERS OF THE SELECTED CC-CV AND MCC-CV CASES.

Cases	I_{CC} (I_{C1})	Δ_{BI}	Δ_I	J_{CT}	J_{BA} [10^{-4}]	J_{EL} [10^3]
CC-CV1	12.531	–	–	750	1.509	1.704
CC-CV2	9.085	–	–	850	1.346	1.491
CC-CV3	7.798	–	–	950	1.251	1.342
MCC-CV1	13.571	1.655	1.405	750	1.517	1.718
MCC-CV2	9.684	1.646	1.146	850	1.359	1.504
MCC-CV3	7.895	1.526	1.026	950	1.255	1.348

are presented in Fig. 11(c). These Pareto curves become single points for both CC-CV and MCC-CV patterns, as observed in Fig. 4. For the case of CC-CV(A) with an initial constant current of 7.504A, the best trade-off point is achieved as $J_{EL} = 1.300 \times 10^3$ and $J_{BA} = 1.226 \times 10^{-4}$. For the case of MCC-CV(B) with $I_{C1} = 7.503A$, $\Delta_{BI} = 1.998A$, and $\Delta_I = 1.497A$, the best trade-off point becomes $J_{EL} = 1.294 \times 10^3$ and $J_{BA} = 1.224 \times 10^{-4}$, which are 0.47% and 0.23% less than those in CC-CV(A). The maximum current decrements are specified for MCC-CV(B), causing the current profile to reduce dramatically at the end of every CC stage. This optimized MCC-CV(B) favors the energy conversion efficiency and battery health but slow down the charging speed; the charging time is 998s, which is 1.7% more than the optimized CC-CV(A).

The evolution profiles of battery capacity loss over charging cycles for the optimized CC-CV(A) and MCC-CV(B) are shown in Fig. 13. For CC-CV(A), the capacity loss increases to 6.29% after 1000 charging cycles, while MCC-CV(B) achieves 5.25% capacity loss, which is 16.5% less than the optimized CC-CV pattern. In summary, relative to CC-CV with the same initial constant current, the MCC-CV pattern is able to slow down the battery degradation but sacrifices some charging speed. This decreased capacity loss rate is mainly

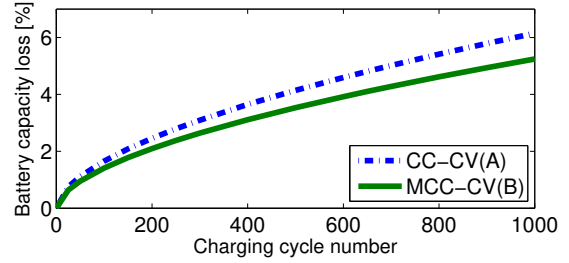


Fig. 13. Evolution of battery capacity loss over charging cycles for CC-CV(A) and MCC-CV(B) charging patterns.

caused by some large stepwise current decrements occurring at the time when the battery terminal voltage reaches its thresholds during the MCC-CV pattern, which will slow down the Li ionic intercalation/de-intercalation process and further reduce unfavorable electrochemical side reactions inside Li-ion battery.

In practice, various charging applications would result in different demand priorities. For home charging, sufficient charging time can be assumed (usually 6-8h) so the priorities in this case become the high energy conversion efficiency and low battery capacity loss. For station charging with the demand of charging batteries within a short period, the priority here would be the fast charging speed. Hence, we can select suitable CC-CV/MCC-CV patterns for different priorities based on the corresponding Pareto frontiers.

E. Further Discussions

This article focuses on the development of a charging pattern optimization framework for Li-ion batteries. The key idea is to search for an optimal balance of different charging preferences by explicitly taking the electrothermal-aging dynamics and health-related constraints into account. Indeed, developing a sufficiently accurate and general battery model including the aging behavior is an open research problem. However, the optimization objectives, constraints, and battery models can be extended or replaced by other proper ones for the same battery or other cell chemistries. Future research work includes experimental validation of the obtained charging patterns and their implementation as a part of battery management systems.

VI. CONCLUSIONS

An innovative model-based strategy has been proposed to enable health-conscious, energy-efficient, fast charging of Li-ion batteries. This is achieved by initially modeling the battery's electrothermal and aging dynamics in two timescales as well as their nonlinear coupling relationships. Then, the objectives in battery aging, charging speed, and energy conversion efficiency are formulated, subject to current, voltage, SOC, and temperature constraints. The highly nonlinear constrained optimization problem is solved by an EM-BBO approach, resulting in suitable CC-CV and MCC-CV patterns for different priorities. With different combinations of charging objectives and sensitive elements, the trade-offs in the sense of Pareto frontier are comprehensively compared and analyzed.

As compared to the health-oriented CC-CV pattern, the corresponding MCC-CV pattern can restrain the capacity loss by over 16% after 1000 charging cycles, while its charging speed for each cycle is sacrificed by nearly 2% accordingly. The proposed charging strategy with Pareto frontiers intends to guide designers to adjust charging patterns for their specific applications.

REFERENCES

- [1] X. Hu, C. Zou, C. Zhang, and Y. Li, "Technological developments in batteries: A survey of principal roles, types, and management needs," *IEEE Power Energy Mag.*, vol. 15, no. 5, pp. 20–31, 2017.
- [2] C. Lv, H. Wang, B. Zhao, D. Cao, W. Huaji, J. Zhang, Y. Li, and Y. Yuan, "Cyber-physical system based optimization framework for intelligent powertrain control," *SAE Int. J. Commercial Veh.*, vol. 10, no. 2017-01-0426, pp. 254–264, 2017.
- [3] C. Lv, Y. Liu, X. Hu, H. Guo, D. Cao, and F.-Y. Wang, "Simultaneous observation of hybrid states for cyber-physical systems: A case study of electric vehicle powertrain," *IEEE Trans. Cybernetics*, 2017.
- [4] K. Liu, K. Li, and C. Zhang, "Constrained generalized predictive control of battery charging process based on a coupled thermoelectric model," *J. Power Sources*, vol. 347, pp. 145–158, 2017.
- [5] Z. Chu, X. Feng, L. Lu, J. Li, X. Han, and M. Ouyang, "Non-destructive fast charging algorithm of lithium-ion batteries based on the control-oriented electrochemical model," *Appl. Energy*, vol. 204, no. 15, pp. 1240–1250, 2017.
- [6] H. Yu, D. Tarsitano, X. Hu, and F. Cheli, "Real time energy management strategy for a fast charging electric urban bus powered by hybrid energy storage system," *Energy*, vol. 112, pp. 322–331, 2016.
- [7] K. Liu, K. Li, H. Ma, J. Zhang, and Q. Peng, "Multi-objective optimization of charging patterns for lithium-ion battery management," *Energy Conversion and Management*, vol. 159, pp. 151–162, 2018.
- [8] S. Pramanik and S. Anwar, "Electrochemical model based charge optimization for lithium-ion batteries," *J. Power Sources*, vol. 313, pp. 164–177, 2016.
- [9] J. Liu, G. Li, and H. K. Fathy, "An extended differential flatness approach for the health-conscious nonlinear model predictive control of lithium-ion batteries," *IEEE Trans. Control Syst. Technol.*, vol. 25, no. 5, pp. 1882–1889, 2017.
- [10] C. Zou, X. Hu, S. Dey, L. Zhang, and X. Tang, "Nonlinear fractional-order estimator with guaranteed robustness and stability for lithium-ion batteries," *IEEE Trans. Ind. Electron.*, vol. 7, no. 65, pp. 5951–5961, 2018.
- [11] C. Zou, C. Manzie, and D. Nešić, "A framework for simplification of PDE-based lithium-ion battery models," *IEEE Trans. Control Syst. Technol.*, vol. 24, no. 5, pp. 1594–1609, 2016.
- [12] A. Abdollahi, X. Han, G. V. Avvari, N. Raghunathan, B. Balasingam, K. R. Pattipati, and Y. Bar-Shalom, "Optimal battery charging, part i: Minimizing time-to-charge, energy loss, and temperature rise for oc-resistance battery model," *J. Power Sources*, 2015.
- [13] H. Perez, X. Hu, S. Dey, and S. Moura, "Optimal charging of li-ion batteries with coupled electro-thermal-aging dynamics," *IEEE Trans. Veh. Technol.*, vol. 66, no. 9, pp. 7761–7770, 2017.
- [14] C. Zou, X. Hu, Z. Wei, and X. Tang, "Electrothermal dynamics-conscious lithium-ion battery cell-level charging management via state-monitored predictive control," *Energy*, vol. 141, pp. 250–259, 2017.
- [15] X. Hu, S. Li, H. Peng, and F. Sun, "Charging time and loss optimization for LiNMC and LiFePO₄ batteries based on equivalent circuit models," *J. Power Sources*, vol. 239, pp. 449–457, 2013.
- [16] C. Zhang, J. Jiang, Y. Gao, W. Zhang, Q. Liu, and X. Hu, "Charging optimization in lithium-ion batteries based on temperature rise and charge time," *Appl. Energy*, vol. 194, pp. 569–577, 2017.
- [17] K. Liu, K. Li, Z. Yang, C. Zhang, and J. Deng, "An advanced lithium-ion battery optimal charging strategy based on a coupled thermoelectric model," *Electrochim. Acta*, vol. 225, pp. 330–344, 2017.
- [18] Q. Ouyang, J. Chen, J. Zheng, and H. Fang, "Optimal multi-objective charging for lithium-ion battery packs: A hierarchical control approach," *IEEE Tran. Ind. Info.*, 2018.
- [19] P. Keil and A. Jossen, "Charging protocols for lithium-ion batteries and their impact on cycle life - an experimental study with different 18650 high-power cells," *J. Energy Storage*, vol. 6, pp. 125–141, 2016.
- [20] M. Abdel-Monem, K. Trad, N. Omar, O. Hegazy, P. Van den Bossche, and J. Van Mierlo, "Influence analysis of static and dynamic fast-charging current profiles on ageing performance of commercial lithium-ion batteries," *Energy*, vol. 120, pp. 179–191, 2017.
- [21] S.-C. Wang and Y.-H. Liu, "A PSO-based fuzzy-controlled searching for the optimal charge pattern of Li-ion batteries," *IEEE Trans. Ind. Electron.*, vol. 62, no. 5, pp. 2983–2993, 2015.
- [22] T. T. Vo, X. Chen, W. Shen, and A. Kapoor, "New charging strategy for lithium-ion batteries based on the integration of Taguchi method and state of charge estimation," *J. Power Sources*, vol. 273, pp. 413–422, 2015.
- [23] H. Ma, D. Simon, P. Siarry, Z. Yang, and M. Fei, "Biogeography-based optimization: a 10-year review," *IEEE Trans. Emerging Top Comput. Intellig.*, vol. 1, no. 5, pp. 391–407, 2017.
- [24] H. Ma, S. Su, D. Simon, and M. Fei, "Ensemble multi-objective biogeography-based optimization with application to automated warehouse scheduling," *Eng. Appl. Artificial Intel.*, vol. 44, pp. 79–90, 2015.
- [25] S. Nejad, D. Gladwin, and D. Stone, "A systematic review of lumped-parameter equivalent circuit models for real-time estimation of lithium-ion battery states," *J. Power Sources*, vol. 316, pp. 183–196, 2016.
- [26] K. Liu, K. Li, Q. Peng, and C. Zhang, "A brief review on key technologies in the battery management system of electric vehicles," *Frontiers of Mechanical Engineering*, pp. 1–18, 2018.
- [27] X. Lin, H. E. Perez, S. Mohan, J. B. Siegel, A. G. Stefanopoulou, Y. Ding, and M. P. Castanier, "A lumped-parameter electro-thermal model for cylindrical batteries," *J. Power Sources*, vol. 257, pp. 1–11, 2014.
- [28] G. Suri and S. Onori, "A control-oriented cycle-life model for hybrid electric vehicle lithium-ion batteries," *Energy*, vol. 96, pp. 644–653, 2016.
- [29] M. Jafari, A. Gauchia, S. Zhao, K. Zhang, and L. Gauchia, "Electric vehicle battery cycle aging evaluation in real-world daily driving and vehicle-to-grid services," *IEEE Trans. Transport. Electrification*, vol. 4, no. 1, pp. 122–134, 2018.
- [30] A. Kamjoo, A. Maheri, A. M. Dizqah, and G. A. Putrus, "Multi-objective design under uncertainties of hybrid renewable energy system using nsga-ii and chance constrained programming," *Int J Electrical Power & Energy Syst.*, vol. 74, pp. 187–194, 2016.
- [31] Q. Kang, S. Feng, M. Zhou, A. C. Ammari, and K. Sedraoui, "Optimal load scheduling of plug-in hybrid electric vehicles via weight-aggregation multi-objective evolutionary algorithms," *IEEE Trans. Intelligent Transport. Syst.*, vol. 18, no. 9, pp. 2557–2568, 2017.
- [32] W. K. Mashwani, A. Salhi, O. Yeniay, H. Hussian, and M. Jan, "Hybrid non-dominated sorting genetic algorithm with adaptive operators selection," *Applied Soft Computing*, vol. 56, pp. 1–18, 2017.



Kailong Liu is a Research Fellow in the Warwick Manufacturing Group, University of Warwick, United Kingdom. He received the B.Eng. degree in electrical engineering and the M.Sc. degree in control theory and control engineering from Shanghai University, China, and the Ph.D. degree in electrical engineering from the Energy, Power and Intelligent Control group, Queen's University Belfast, United Kingdom, in 2011, 2014, and 2018, respectively.

He was a Visiting Student Researcher at the Tsinghua University and the North China Electric Power University, China, in 2016. His research interests include modeling, optimization and control with applications to electrical/hybrid vehicles, energy storage, and battery management system.

Dr. Liu was the student chair of IEEE QUB student branch and a recipient of awards such as EPSRC Scholarship, Santander International Scholarship, and QUB ESM International Scholarship.



Kang Li (M'05-SM'11) received the B.Sc. degree in Industrial Automation from Xiangtan University, Hunan, China, in 1989, the M.Sc. degree in Control Theory and Applications from Harbin Institute of Technology, Harbin, China, in 1992, and the Ph.D. degree in Control Theory and Applications from Shanghai Jiaotong University, Shanghai, China, in 1995. He was also awarded the D.Sc. degree in Science from Queen's University Belfast, UK, in 2015.

Between 1995 and 2018, he worked at Shanghai Jiaotong University, Delft University of Technology and Queen's University Belfast as a research fellow. Between 2002 and 2018, he was a Lecturer, a Senior Lecturer (2007), a Reader (2009) and a Chair Professor (2011) with the School of Electronics, Electrical Engineering and Computer Science, Queen's University Belfast, Belfast, U.K. He currently holds the Chair of Smart Energy Systems at the University of Leeds, UK. His research interests covers nonlinear system modeling, identification, and control, and bio-inspired computational intelligence,



Changfu Zou (M'16) is a Postdoctoral Fellow in the Department of Electrical Engineering, Chalmers University of Technology, Sweden. He received the B.E. degree in Automotive Engineering from Beijing Institute of Technology, China, in 2011, and the Ph.D. degree in Automation and Control Engineering from the Department of Mechanical Engineering, The University of Melbourne, Australia, in 2017.

He was a Visiting Student Researcher at the Energy, Controls, & Applications Lab, University of California, Berkeley, USA, between 2015 and 2016. His research interests include modeling, state/parameter estimation, and control with application to energy storage systems and electric vehicles. His current research projects are supported by Swedish Energy Agency and Volvo Cars. Dr. Zou was a recipient of awards such as Excellent Graduate of Beijing, Melbourne Research Scholarship, NICTA Scholarship, and Engineering & IT Melbourne Abroad Travel Scholarships.

with applications to energy and power systems, smart grid, electric vehicles, and energy management in industrial sectors. He has authored/co-authored over 100 journal publications, and edited/co-edited over 10 conference proceedings.

Dr Li chairs the IEEE UKRI Control and Communication Ireland chapter, and was the Secretary of the IEEE UK and Ireland Section. He is a visiting professor of Queen's University Belfast, Shanghai Jiaotong University, Tianjin University, Chongqing University, Shanghai University, Hangzhou Dianzi University, and Ningbo Institute of Technology of Zhejiang University. He also previously held visiting fellowship or visiting professorship at National University of Singapore, University of Iowa, New Jersey Institute of Technology, Tsinghua University, Technical University of Bari, Taranto, and Harbin Institute of Technology.



Torsten Wik received the M.Sc. degree in chemical engineering (majoring in applied mathematics), the Licentiate of Engineering degree in control engineering, the Ph.D. degree in environmental sciences (majoring in automatic control), and the Docent degree in electrical engineering from the Chalmers University of Technology, Gothenburg, Sweden, in 1994, 1996, 1999, and 2004, respectively.

He worked as a Senior Researcher at Volvo Technology, Gothenburg, in control system design for combustion engine test cells, and combined reformer and fuel cells, from 2005 to 2007. He is a Professor and the Head of Automatic Control with the Department of Electrical Engineering, Chalmers University of Technology. His current research interests include optimal control, model reduction, and systems with model uncertainties, with applications to energy storage, environmental, and biological systems. Professor Wik serves as an Associate Editor for Elsevier Control Engineering Practice.